Citron kinase mediates transition from constriction to abscission through its coiled-coil domain

Sadanori Watanabe[1,2,*], Tihana De Zan[1,3], Toshimasa Ishizaki[1] and Shuh Narumiya[1,*]

[1]Department of Pharmacology, Kyoto University Faculty of Medicine, Kyoto 606-8501, Japan
[2]Division of Biological Science, Graduate School of Science, Nagoya University, Furo-cho, Chikusa-ku, Nagoya 464-8602, Japan
[3]Division of Molecular Biology, Ruđer Bošković Institute, Bijenička cesta 54, 10000 Zagreb, Croatia
*Authors for correspondence (snaru@mfour.med.kyoto-u.ac.jp; sadanori.watanabe@bio.nagoya-u.ac.jp)

Accepted 4 February 2013
Journal of Cell Science 126, 1773–1784
© 2013. Published by The Company of Biologists Ltd
doi: 10.1242/jcs.116608

Summary

Cytokinesis is initiated by constriction of the cleavage furrow, and completed with separation of the two daughter cells by abscission. Control of transition from constriction to abscission is therefore crucial for cytokinesis. However, the underlying mechanism is largely unknown. Here, we analyze the role of Citron kinase (Citron-K) that localizes at the cleavage furrow and the midbody, and dissect its action mechanisms during this transition. Citron-K forms a stable ring-like structure at the midbody and its depletion affects the maintenance of the intercellular bridge, resulting in fusion of two daughter cells after the cleavage furrow ingression. RNA interference (RNAi) targeting Citron-K reduced accumulation of RhoA, Anillin, and septins at the intercellular bridge in mid telophase, and impaired concentration and maintenance of KIF14 and PRC1 at the midbody in late telophase. RNAi rescue experiments revealed that these functions of Citron-K are mediated by its coiled-coil (CC) domain, and not by its kinase domain. The C-terminal part of CC contains a Rho-binding domain and a cluster-forming region and is important for concentrating Citron-K from the cleavage furrow to the midbody. The N-terminal part of CC directly binds to KIF14, and this interaction is required for timely transfer of Citron-K to the midbody after furrow ingression. We propose that the CC-domain-mediated translocation and actions of Citron-K ensure proper stabilization of the midbody structure during the transition from constriction to abscission.

Key words: Cytokinesis, Abscission, Midbody

Introduction

During cytokinesis, the cleavage furrow is formed in the middle region of a dividing cell, and ingression of the furrow results in formation of the intercellular bridge containing an electron-dense structure called the midbody. The midbody forms at the central part of the intercellular bridge where antiparallel arrays of microtubules overlap. This structure is maintained until the daughter cells are physically separated by the final cytokinetic process called abscission. Series of studies have revealed that the formation and ingression of the cleavage furrow are carried out by the actomyosin contractile machinery (Eggert et al., 2006; Pollard, 2010), and the abscission is carried out by the combination of several events including vesicle trafficking, microtubule remodeling and membrane deformation (Barr and Gruneberg, 2007; Steigemann and Gerlich, 2009; Neto and Gould, 2011). While the mechanism of both the constriction and abscission has been analyzed and actions of key molecules therein have been identified, it is still poorly understood how constriction and abscission are coupled, which molecules mediate this transition and how they act (Hu et al., 2012). Among molecules that localize at the contractile ring and the midbody is the small GTPase Rho. It is activated at the equatorial cell cortex, and exerts its functions by mobilizing Rho effectors (Piekny et al., 2005; Narumiya and Yasuda, 2006). One of the Rho effectors mobilized by active Rho, Citron kinase (Citron-K), localizes at the central spindle, and is transferred to the cleavage furrow in a Rho-dependent manner, and accumulates at the midbody as a ring-like structure (Madaule et al., 1998; Eda et al., 2001). Citron-K is a multiple domain protein containing an N-terminal kinase domain, an internal coiled-coil (CC) domain with Rho/Rac interacting site, and a C-terminal region consisting of a Zn finger, a pleckstrin homology (PH) domain, a Citron homology domain (CNH), a putative SH3 binding domain, and a PDZ-targeting motif (Di Cunto et al., 1998; Madaule et al., 2000; Yamashiro et al., 2003). Citron-K or its fly orthologue Sticky has been suggested to interact with several molecules in cytokinesis such as Kinesin-3 KIF14 (Gruneberg et al., 2006), ASPM (Paramasivam et al., 2007), actin, myosin light chain (Bassi et al., 2011) and Anillin (Gai et al., 2011). Although Citron-K/Sticky has been shown essential in cytokinesis *in vitro* in cultured cells (Echard et al., 2004; Gruneberg et al., 2006) and *in vivo* (Di Cunto et al., 2000; Cunto et al., 2002; D'Avino et al., 2004; Naim et al., 2004; Shandala et al., 2004), it has not been fully elucidated how Citron-K is localized in the midbody, which domains mediate its localization, and how and in which phase of cytokinesis each domain functions critically. To clarify these issues, we have used RNA interference (RNAi) combined with live cell imaging and examined molecular dynamics of Citron-K and effect of its depletion on cytokinesis. We have then performed a series of domain-based RNAi rescue experiments and identified regions of Citron-K critical in its localization and function during cytokinesis. We have next examined molecular interactions with the identified domains of Citron-K and analyzed roles of these interactions in the Citron-K function. Here, we

Journal of Cell Science

show that the Citron-K function in cytokinesis is mainly mediated by its CC domain, which alone stabilizes the midbody structure until abscission. We also show that CC domain is required for the interaction with KIF14, and that this interaction enables transfer of Citron-K to the midbody upon full ingression of the furrow.

Results

Depletion of Citron-K impairs maintenance of the midbody

We depleted Citron-K in HeLa cells with three non-overlapping siRNAs. Citron-K RNAi increased the number of multinucleate cells 48 hours after transfection (supplementary material Fig. S1A). Videomicroscopy using HeLa cells stably expressing EGFP-α-tubulin (EGFP-tub HeLa cells) showed that the cytokinesis failure of Citron-K-depleted cells with either siRNA occurred after full ingression of the cleavage furrow (Fig. 1), which is consistent with previous reports (Echard et al., 2004; Gai et al., 2011). We measured the time from completion of cleavage furrow ingression to cytokinesis failure in Citron-K RNAi cells and compared its distribution with distributions of time of asymmetric microtubule disassembly and final disconnection of daughter cells in control RNAi cells (Fig. 1A). Among the Citron-K RNAi cells with cytokinesis failure, 80% exhibited the failure around 60 minutes after full ingression before the peak of microtubule disassembly in control cells, while the rest failed cytokinesis from 140 to 200 minutes after full ingression, which was after the peak of abscission in control cells (Fig. 1A). Notably, microtubule disassembly was not seen in any of Citron-K RNAi cells with cytokinesis failure (data not shown and see later). Following Gai et al. (Gai et al., 2011), we call the former 'early fusion' and the latter 'late fusion'. We then characterized modes of failure in early and late fusion (Fig. 1B–D; supplementary material Movies 1–3). In cells undergoing 'early fusion', two daughter cells are connected with a shorter intercellular bridge, and do not separate well. As the midbody microtubules were displaced from the center toward

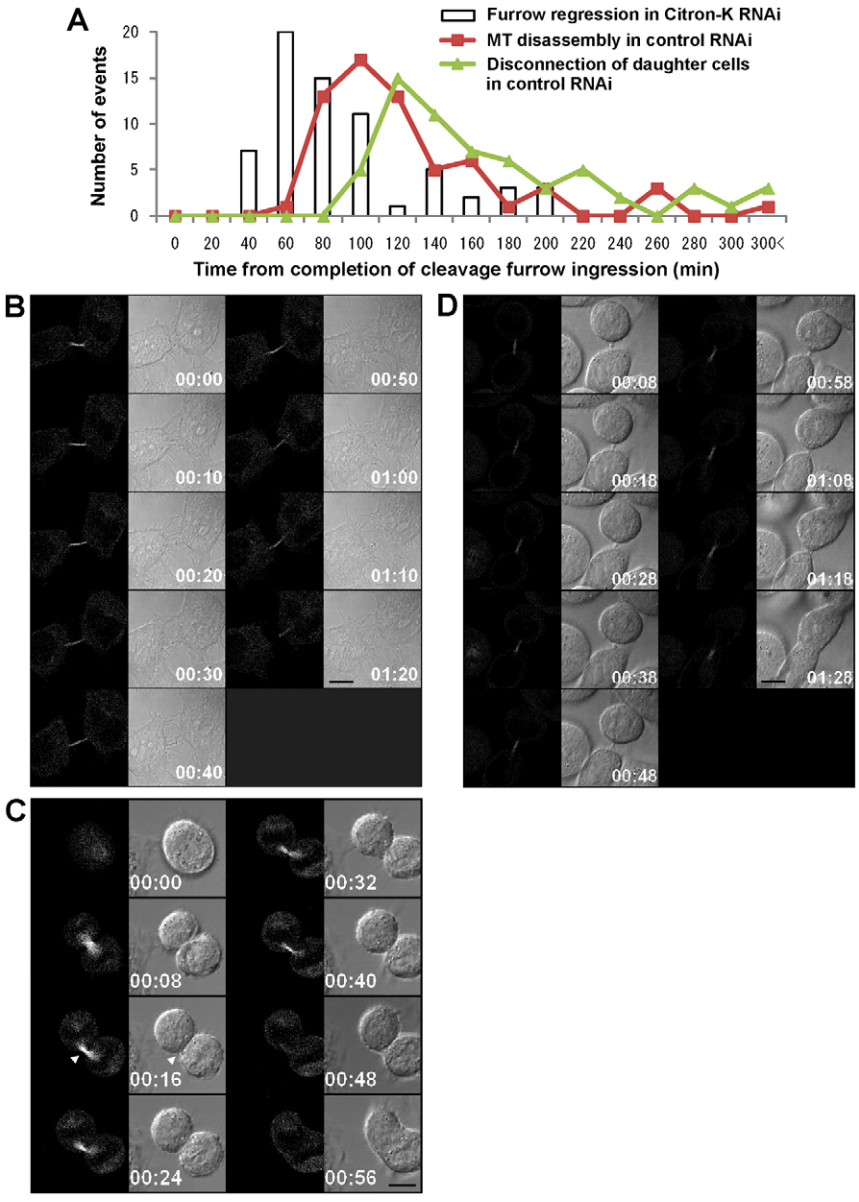

Fig. 1. Depletion of Citron-K induced cytokinesis failure after cleavage furrow ingression. (**A**) Distribution of time of cytokinesis failure after completion of furrow ingression in Citron-K RNAi cells. EGFP-tub HeLa cells were synchronized with thymidine and subjected to control or Citron-K RNAi as described in Materials and Methods. Mitotic cells enriched at 33 hours after RNAi transfection were imaged every 4 minutes for another 6 hours. Time from complete furrow ingression to cytokinesis failure in Citron-K RNAi cells (n=70), and timing of asymmetric microtubule disassembly and disconnection of daughter cells in control RNAi cells (n=66, 63, respectively) were measured. (**B–D**) Time-lapse video images of EGFP-tub HeLa cells subjected to control (B and supplementary material Movie 1) or Citron-K RNAi (C,D; supplementary material Movies 2 and 3). EGFP-tub HeLa cells were synchronized and transfected as described for A, and the cells in mitosis at 35 hours after RNAi transfection were subjected to time-lapse video microscopy. Time-lapse video frames for EGFP-tubulin (left columns) and for DIC (right columns) were selected every 8 minutes (C) or 10 minutes (B,D). C shows early cytokinesis failure and D shows late cytokinesis failure in Citron-K RNAi cells. Arrowheads indicate formation of the midbody. Scale bar: 10 μm.

Journal of Cell Science

either of the two daughter cells, the two cells fused with the microtubules absorbed into that daughter cell (Fig. 1C; supplementary material Movie 2). In 'late fusion', two daughter cells are connected with an intercellular bridge of the length comparable to that in control cells. The fusion of these cells began when the plasma membrane covering the midbody detached from the underlying microtubule structure, resulting in fusion of the two cells into one (Fig. 1D; supplementary material Movie 3). Movie 3 shows that the midbody is formed in Citron-K RNAi cells as in control cells, and that it is getting less clear in buldging and finally disappears in Citron-K RNAi cells. These results suggest that Citron-K is important to keep proper structure of the midbody which holds the intercellular bridge microtubules between the two daughter cells and is thus required for successful transition from constriction to abscission.

Citron-K concentrates to the midbody as a stable ring-like structure and is required for maintenance of Rho, Anillin and septins

We expressed EGFP-tagged full-length (FL) Citron-K in HeLa cells, and examined its behavior during cytokinesis (Fig. 2A). EGFP-Citron-K first appeared at the equatorial cortex in anaphase, concentrated at the cleavage furrow in early telophase, accumulated in the middle of the intercellular bridge with full ingression of the cleavage furrow in mid telophase (t=00:00), and formed a ring-like structure in the midbody in late telophase (Fig. 2A; supplementary material Movie 4). Fluorescence recovery after photobleaching (FRAP) analysis revealed that recovery of EGFP-Citron-K was observed within 100 seconds with photobleaching of Citron-K at the equatorial cortex in anaphase, whereas the recovery was not detected during this period when Citron-K at the midbody was photobleached (Fig. 2B; supplementary material Fig. S1B,C). Similar negligible turnover was also observed when we photobleached a half of the EGFP-Citron-K signals at the midbody (data not shown).

We next examined effects of Citron-K depletion on localization of RhoA, Anillin and septins in mid–late telophase. RhoA is a binding partner of Citron-K and *Drosophila* homologs of the latter two molecules were suggested important in maintenance of the midbody (Madaule et al., 2000; Echard et al., 2004; Naim et al., 2004). RhoA was concentrated from the cleavage furrow to the intercellular bridge in mid telophase, and became negligible in late telophase (supplementary material Fig. S2A). Anillin was also concentrated from the cleavage furrow to the intercellular bridge in mid telophase, and then localized in the stem of the bridge in late telophase (Fig. 2C, right panels). Septin signals, as examined by localization of endogenous septin 6 and septin 7, were observed on the intercellular bridge in mid

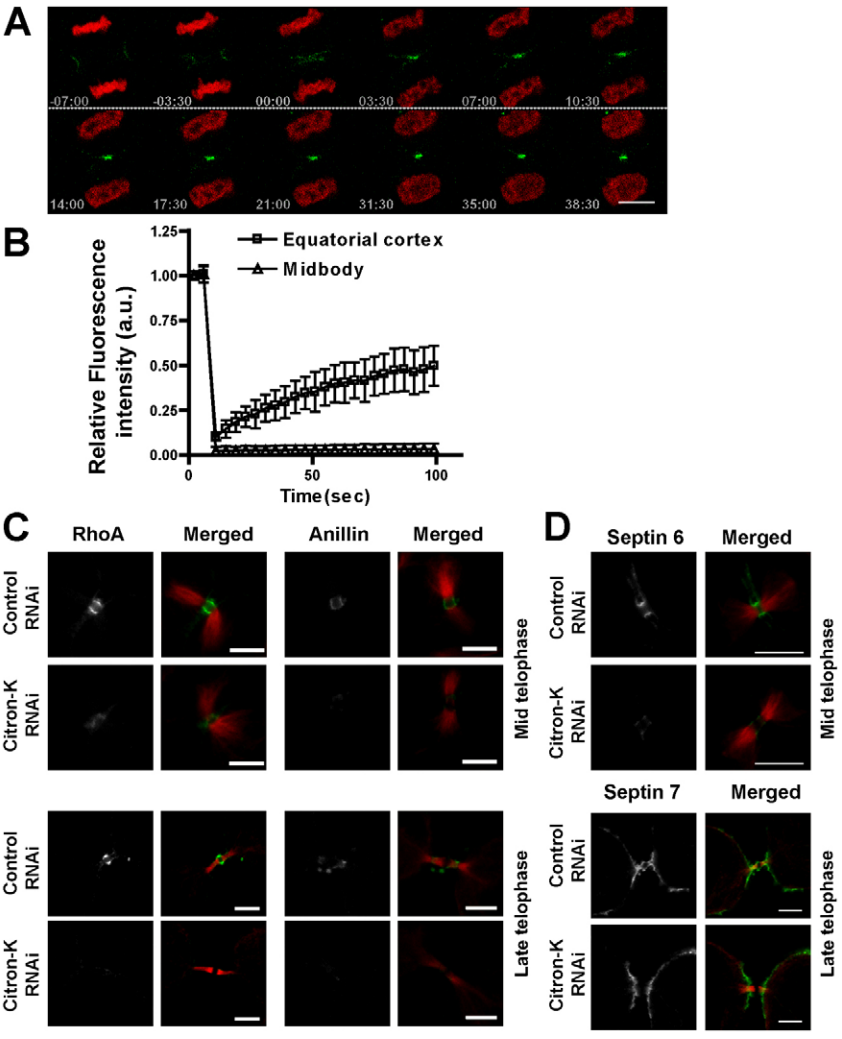

Fig. 2. Localization and dynamics of Citron-K in cytokinesis and effects of its depletion on localization of Rho, Anillin and septins in telophase. (**A**) Time-lapse video image of a HeLa cell expressing EGFP-Citron-K during cytokinesis. HeLa cells were transfected with EGFP-Citron-K FL (green) and DsRed-Histone H2Bk (red), and the cells in mitosis were subjected to video microscopy (supplementary material Movie 4). A typical example is shown. (**B**) FRAP analysis of GFP-Citron-K in the equatorial cell cortex and the midbody. Experiments were performed as described in supplementary material Fig. S1B. Relative fluorescence intensities of GFP-Citron-K at bleached regions in the equatorial cell cortex and the midbody were obtained from 10 cells of each group. Error bars represent s.d. (**C**,**D**) Effects of Citron-K depletion on localization of RhoA, Anillin and septins in telophase. HeLa cells were synchronized and subjected to control or Citron-K RNAi as described in Materials and Methods, and 32 hours after transfection the cells were further synchronized in mitosis by treatment with 20 ng/ml of nocodazole for another 4 hours. The cells were washed and cultured in fresh medium for 60 minutes (upper columns) or 90 minutes (bottom columns), fixed and stained for α-tubulin (red) and indicated molecules (green). Immunofluorescence for RhoA, Anillin (C) and septins (D) in mid and late telophase is shown. Scale bars: 10 μm (A), 5 μm (C,D).

telophase, and became patchy in late telophase (Fig. 2D). Citron-K co-localized with these three molecules in early to mid telophase (Fig. 2A,C,D). Depletion of Citron-K did not affect their accumulation in the cleavage furrow in early telophase (data not shown), but impaired their accumulation in the intercellular bridge in mid–late telophase (Fig. 2C,D; supplementary material Fig. S2B). These results suggest that Citron-K maintains localization of Rho, Anillin and septins in the intercellular bridge.

Citron-K is required for focused concentration and maintenance of microtubule-associated proteins, KIF14 and PRC1, at the midbody

Since microtubules are the basic component of the midbody, we next examined the effect of Citron-K depletion on microtubule-associated proteins at the midbody. We first examined the localization of MKLP1/KIF23, one of the core components of the midbody (Guse et al., 2005). MKLP1 localized in the midbody similarly in control and Citron-K RNAi cells (supplementary material Fig. S3A,B). We next examined localization of KIF14, a candidate for a Citron-K-interacting protein in cytokinesis (Gruneberg et al., 2006), by both immunofluorescence and expression of GFP-KIF14. By immunofluorescence, KIF14 localized at the outer region of the midbody as two foci at earlier time points and accumulated in the midbody at later time points in control cells (supplementary material Fig. S3C) (Fig. 3A, panel 1). These immunofluorescence signals were verified by KIF14 RNAi (supplementary material Fig. S3D). On the other hand, the KIF14 signals were found at the outer region of the midbody in Citron-K RNAi cells even in the later time points (Fig. 3A, panel 2). However, GFP-KIF14 as examined by GFP fluorescence was seen as a continuous signal covering the midbody from the outer to inner regions in Citron-K RNAi cells (Fig. 3A, panel 4). We therefore examined the immunofluorescence of KIF14 antibodies in GFP-KIF14 expressing cells. Anti-KIF14 signals were seen as two foci at the outer region in Citron-K RNAi cells expressing GFP-KIF14 (Fig. 3A, panel 6), while GFP signals and anti-KIF14 signals both showed a focused band in the midbody in control RNAi cells (Fig. 3A, panels 3, 5). When the GFP-KIF14 localization was examined by GFP antibody, anti-GFP signals in Citron-K RNAi cells were found again as two foci at the outer region of the midbody similar to KIF14 antibody (data not shown). These results therefore suggest that KIF14 fails to accumulate focally in the central region of the midbody in Citron-K RNAi cells. Indeed, expression of GFP-Citron-K recovered the KIF14 immunofluorescence in the midbody in late telophase (supplementary material Fig. S3E). The failure to detect KIF14 in the core of the midbody by immunofluorescence in Citron-K RNAi cells could be due to difference of antibody accessibility to the KIF14 epitope at the midbody between control and Citron-K RNAi cells. Since Gruneberg et al. (Gruneberg et al., 2006) previously showed that KIF14 interacts with PRC1 at the midbody, we next examined effect of Citron-K depletion on localization of PRC1 at the midbody. Using mCherry-PRC1 (Subramanian et al., 2010; Elad et al., 2011), we observed that PRC1 accumulated at the midbody in control cells throughout telophase until abscission (Fig. 3B, top; supplementary material Movie 5), while the PRC1 signals, once accumulated in the midbody as in control cells, were gradually dispersed from there in Citron-K RNAi cells (Fig. 3B, bottom; supplementary material

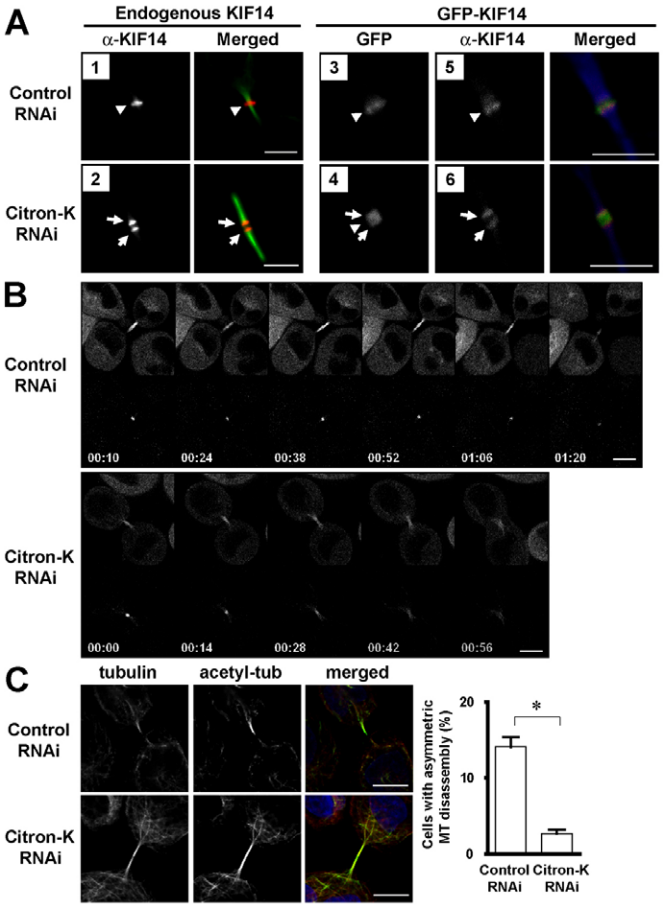

Fig. 3. Citron-K is required for focused concentration of KIF14 and PRC1 and asymmetrical disassembly of the midbody microtubules. (**A**) Effects of Citron-K depletion on KIF14 localization in cytokinesis. HeLa cells were synchronized, transfected and enriched in mitosis as described for Fig. 2C. The cells were cultured for 120 minutes after nocodazole release, fixed and subjected to immunofluorescence analysis (left). Immunofluorescence for KIF14 (red) and α-tubulin (green) in control and Citron-K RNAi cells is shown. In a separate experiment, cells were transfected with GFP-KIF14 after the 2nd thymidine release, cultured as described above, and stained for KIF14 and α-tubulin (right). Localization of the GFP signal of GFP-KIF14 (green) is compared with the immunofluorescence signals of KIF14 (red) and α-tubulin (blue). Arrowheads and arrows indicate the localization of KIF14 in the inner and outer region of the midbody, respectively. (**B**) Effects of Citron-K depletion on dynamics of PRC1 at the midbody. EGFP-tub HeLa cells were synchronized and transfected with mCherry-PRC1 as described in Materials and Methods. The cells in telophase were subjected to time-lapse video microscopy as described for Fig. 1B. Time-lapse video images of cells expressing EGFP-tubulin (top) and mCherry-PRC1 (bottom) were selected every 14 minutes from supplementary material Movie 5 of control RNAi cells (upper panels) and supplementary material Movie 6 of Citron-K RNAi cells (lower panels). (**C**) Effects of Citron-K depletion on asymmetric disassembly of the midbody microtubules. Experiments were performed as described in Fig. 3A, and cells in late telophase were permeabilized, fixed and stained for α-tubulin (red), acetylated-tubulin (green) and DNA (blue). Typical examples are shown on the left and percentages of late telophase cells with asymmetric microtubule disassembly are shown on the right. Results were analyzed by Mann–Whitney *U*-test. Error bars indicate s.e.m.; $*P<0.05$. Scale bars: 5 μm (A), 10 μm (B,C).

Movie 6). These results suggest that Citron-K controls the maintenance of PRC1 at the midbody, though we cannot exclude a possibility that the PRC1 dispersion is secondary to the midbody disintegration.

We next examined effects of Citron-K depletion on recruitment of the ESCRT complex components (Caballe and Martin-Serrano, 2011). Cep55, as examined with EGFP-Cep55, localized onto the midbody in late telophase in control and Citron-K RNAi cells (supplementary material Fig. S3F, left), and Cep55 depletion did not affect Citron-K localization in the midbody (supplementary material Fig. S3G). CHMP4B, a core ESCRT-III subunit, localized to two narrow cortical rings adjacent to the midbody in control cells and was diminished by depletion of Cep55, as shown in previous reports (Lee et al., 2008; Guizetti et al., 2011), and this localization was not affected by Citron-K RNAi (supplementary material Fig. S3F, middle). A downstream molecule of ESCRT pathway, Spastin, also localized at the midbody similarly in both control and Citron-K RNAi cells (supplementary material Fig. S3, right). These results suggest that Citron-K and the ESCRT molecules are independently targeted to the midbody. We then wondered if the ESCRT-Spastin pathway functions normally in Citron-K RNAi cells. Since it drives asymmetric disassembly of the midbody microtubules during abscission, we examined intercellular bridge microtubules in the late telophase with antibodies to α-tubulin and acetylated tubulin (Fig. 3C, left). The population that showed asymmetric microtubule disassembly at the particular time point was significantly lower in Citron-K RNAi cells than in control cells (Fig. 3C, right). These results suggest that the ESCRT-Spastin pathway does not function properly in Citron-K RNAi cells.

Identification of the domains responsible for Citron-K function in cytokinesis

The above results suggest that proper functioning of Citron-K at the midbody is important for cytokinesis. To dissect molecular mechanisms of Citron-K action, we first defined the domains of Citron-K responsible for its localization during cytokinesis. We expressed a series of EGFP-Citron-K deletion constructs in HeLa cells depleted of endogenous Citron-K and examined their localization during cytokinesis (Fig. 4A,B). While neither the N-terminal fragment (1–428 aa) containing the kinase domain nor the C-terminal fragment (1354–2055 aa) localized at the cleavage furrow or the midbody (data not shown), the CC domain localized at the cleavage furrow and the midbody (Fig. 4B). We then divided the CC domain into the N-terminal part (CCf, 429–835 aa) and the C-terminal part (CCr, 835–1354 aa) using the score of a coiled-coil prediction software 'Coils Server', and examined their localizations (Fig. 4A,B). We found that CCr localized at the cleavage furrow and the midbody, while CCf localized at the central spindle in early telophase and on outer region of the midbody in late telophase (Fig. 4B). These results suggest that distinct regions of Citron-K CC domain differentially regulate the localizations of Citron-K during cytokinesis. To evaluate the contribution of each domain in cytokinesis, we next performed a rescue experiment of adding EGFP-tagged mouse Citron-K FL, CC, CCf or CCr back to cells depleted of endogenous Citron-K and evaluated their phenotypes (Fig. 4C). In this experiment, we expressed these constructs with a partially deleted CMV promoter (Watanabe, 2012) to get expression level of Citron-K transgene comparable to that of endogenous Citron-K as evidenced by Western blot for

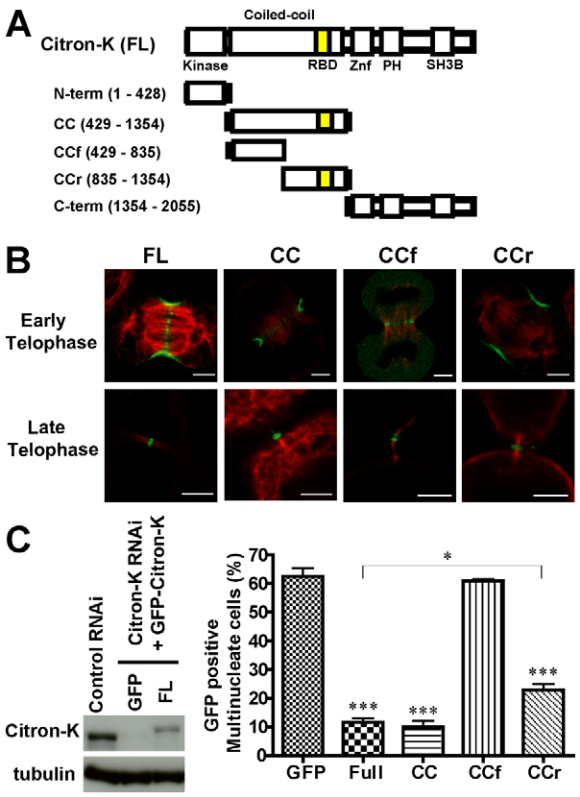

Fig. 4. Identification of Citron-K domains responsible for its localization and function in cytokinesis. (**A**) Representation of domain structure of Citron-K and its fragments. Kinase, kinase domain; RBD, Rho binding domain; Znf, Zn finger domain; PH, pleckstrin homology domain; SH3B, putative SH3-binding domain. (**B**) Localization of Citron-K fragments (CC, CCf, and CCr) in early and late telophase. HeLa cells were synchronized and transfected with siRNACitron-K#1 as described for Fig. 1B. The cells were then transfected after the 2nd thymidine block with either empty GFP vector, pΔCMV-EGFP-Citron-K-FL, CC, CCf or CCr. The transfected cells were washed and released for 11 hours and then subjected to immunofluorescence for GFP (green) and α-tubulin (red). Scale bars: 5 μm. (**C**) Rescue by Citron-K FL or fragments of cytokinesis failure in Citron-K RNAi cells. HeLa cells were synchronized, subjected to RNAi and transfected with pΔCMV-EGFP vectors as described above. The cells were cultured for 16 hours, and the percentage of multinucleate cells per total cells expressing GFP was determined in each group. The graph shows the mean of more than three independent experiments, in each of which $n>100$ cells were examined. Expression of pΔCMV-EGFP-Citron-K-FL was examined by immunoblotting of transfected cells after 11 hours of culture (left). Results were analyzed by one-way ANOVA with the Tukey–Kramer multiple comparison test. Error bars indicate s.e.m.; $^{***}P<0.001$ versus GFP, $^{*}P<0.05$.

GFP-Citron-K FL (Fig. 4C, left). Compared to control Citron-K-RNAi cells expressing GFP alone, significant reduction of binucleation was observed in cells expressing EGFP-Citron-K FL (Fig. 4C, right). Expression of Citron-K CC domain also significantly rescued the cytokinesis failure induced by Citron-K-RNAi (Fig. 4C; supplementary material Fig. S4A). Intriguingly, reduction of the Citron-K RNAi phenotype by Citron-K CC domain was comparable to that of Citron-K FL (Fig. 4C). Of the two CC fragments, the expression of CCf did not correct the Citron-K RNAi phenotype, while that of CCr significantly recovered the cytokinesis failure, though in lesser extent than Citron-K FL expression (Fig. 4C; supplementary material Fig.

S4A,B). Consistently, a Citron-K FL construct lacking CCr (ΔCCr) did not rescue the cytokinesis failure (supplementary material Fig. S4C). These results suggest that the function of Citron-K in cytokinesis is mainly mediated by its CC domain, and that its kinase domain is dispensable in this action. The fact that CCr did not fully reproduce the rescuing effect of CC or FL further suggests that not only CCr but also CCf contribute to the function of Citron-K in cytokinesis.

CCr mediates localization of Citron-K in the cleavage furrow and cluster formation

Since the CCr domain by itself can localize at the midbody and significantly rescue the loss of Citron-K in cytokinesis (Fig. 4C), we next examined the functions of CCr subdomains. The CCr domain contains three potential Rho-binding regions, RID (Rho interacting domain), HR1 (homology region), and RBD (Rho GTPase binding domain) (Blumenstein and Ahmadian, 2004; Serres et al., 2012). Since, among these, RBD shows high homology to that of ROCK, another Rho effector (Madaule et al., 1998) (supplementary material Fig. S5A), we focused on this particular region and examined its function in cytokinesis. We constructed two CCr fragments; CCrΔC1 (835–1248 aa), a CCr fragment with deletion of RBD and its C-terminal part, and CCr-L1263N, a CCr with a point mutation in the amino acid supposed to constitute the interface with GTP-Rho by the analogy of the RBD of ROCK (Shimizu et al., 2003; Dvorsky et al., 2004). CCr-L1263N actually showed impaired Rho-binding activity *in vitro* (supplementary material Fig. S5A,B). While CCr localized exclusively in the cleavage furrow, both CCrΔC1 and CCr-L1263N exhibited more signals in the cytoplasm (Fig. 5A,B). Consequently, localization of these mutants in the intercellular bridge was further attenuated with ingression (Fig. 5C), suggesting that Rho-binding activity is important for localization of Citron-K from the cleavage furrow to the intercellular bridge. Notably, expression of EGFP-Citron-K CCr but not CCrΔC1 or CCr-L1263N significantly restored the signals of RhoA, Anillin, and septin 6 in Citron-K RNAi cells in intercellular bridge in mid telophase (Fig. 5C; supplementary material Fig. S5D; Fig. S6). These results suggest that Citron-K localizes at the midbody by its binding to Rho, and maintains RhoA, Anillin, and septins at the intercellular bridge through this interaction.

We then performed rescue experiments in Citron-K RNAi cells with CCrΔC1 or CCr-L1263N. These mutants exhibited indeed attenuated recovery compared to CCr, but they still showed significant recovery of cytokinesis failure (Fig. 5D). We therefore suspected an additional functional domain in CCrΔC1, and examined localization and activity of a shorter CCr fragment (835–1089 aa), CCrΔC2 (Fig. 5A). While CCrΔC2 exhibited the

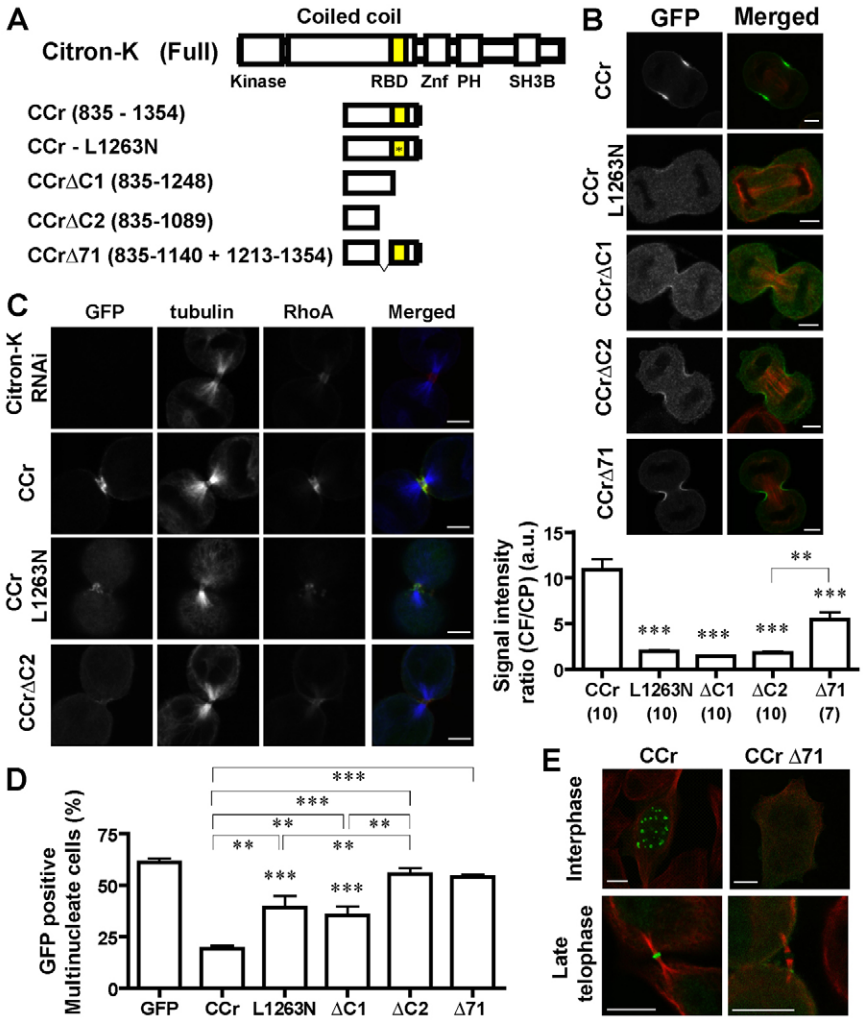

Fig. 5. Citron-K CCr domain exerts essential functions of Citron-K in cytokinesis.
(**A**) Representation of CCr and its mutants. Kinase, kinase domain; RBD, Rho binding domain; Znf, Zn finger domain; PH, pleckstrin homology domain; SH3B, putative SH3-binding domain. (**B**) Localization of CCr mutants in early telophase of Citron-K depleted HeLa cells. HeLa cells were synchronized and transfected with a series of pΔCMV-EGFP-Citron-K constructs (CCr, CCrL1263N, CCrΔC1, CCrΔC2, CCrΔ71) and cells in early telophase were stained for GFP (green) and α-tubulin (red) (top). Fluorescence intensities for GFP at the cytoplasm (CP) and cleavage furrow (CF) were quantified as described in Materials and Methods (bottom). Values indicate CF/CP ratios of each group from two different experiments. Results were analyzed by Tukey–Kramer multiple comparison test. Error bars indicate s.e.m.; ***P<0.001 versus CCr, **P<0.01. The number of cells examined is shown at the bottom of the graph. (**C**) Localization of CCr mutants in mid telophase and their effects on RhoA localization. The cells transfected as above were further enriched in mid telophase, and stained for GFP (green), α-tubulin (blue) and RhoA (red). (**D**) Rescue of cytokinesis failure with Citron-K CCr mutants. Experiments were performed as described in Fig. 4C with a series of pΔCMV-EGFP-Citron-K constructs as above. Values indicate percentages of multinucleate cells per total cells expressing GFP. The graph shows the mean of more than three independent experiments, in each of which n>100 cells were examined. Error bars, s.e.m. ***P<0.001 versus GFP and **P<0.01 by Tukey–Kramer multiple comparison test. (**E**) Cluster formation of GFP-Citron-K CCr and CCrΔ71 in interphase Citron-K-depleted cells. Their localization during late telophase is shown in lower panels. Experiments were performed as described in Fig. 4B,C, and the cells were stained for GFP (green), α-tubulin (red). Scale bars: 5 μm (B,C), 10 μm (E).

Journal of Cell Science

localization in the cleavage furrow, albeit attenuated, this construct exhibited only negligible localization in the midbody (Fig. 5B,C), and showed no significant recovery of cytokinesis failure in the Citron-K-RNAi cells (Fig. 5D).

Citron-K, when overexpressed in cultured cells, makes self-aggregates (Eda et al., 2001), which are called 'clusters' by Zhang and Benson (Zhang and Benson, 2006). We found that CCr made clusters in interphase cells as EGFP-Citron-K FL (Fig. 5E, top; supplementary material Fig. S7A, left), and, by FRAP, that these clusters showed negligible turnover as in the midbody (Fig. 2B; supplementary material Fig. S7A, right). Notably, such clusters were observed in cells expressing EGFP-Citron-K CCr or CCrΔC1, but not in cells expressing CCrΔC2 (data not shown). These results suggest that 1090–1248 a.a. contains a region, which mediates cluster formation and is important for the localization and function of Citron-K in the midbody. A BLAST search found this region to be conserved among Citron-K homologs and homologous to a supposed cluster-forming region in ZEN-4/MKLP1 (supplementary material Fig. S7B) (Hutterer et al., 2009). We therefore constructed a CCr fragment lacking this region, Citron-K CCrΔ71, and examined its localization and function in Citron-K RNAi cells. Although CCrΔ71 localized at the cleavage furrow, this fragment did not accumulate at the midbody (Fig. 5B,E, bottom). CCrΔ71 neither produced GFP-positive clusters in interphase cells nor rescued the Citron-K RNAi phenotype (Fig. 5D,E, top). Taken together, Citron-K CCr contains two important subdomains, the first for targeting and the second for clustering of Citron-K at the midbody.

CCf directly binds KIF14 and regulates its localization

The lack of complete rescue by the CCr expression in Citron-K RNAi cells prompted us to examine CCf as another key domain for Citron-K localization and function (Fig. 4C). Given the localization of CCf at the central spindle and the midbody microtubules (Fig. 4B), we suspected possible co-localization of CCf and KIF14 in Citron-K RNAi cells. Indeed, indirect immunofluorescence study showed colocalization of CCf and KIF14 at the outer regions of the midbody (supplementary material Fig. S8A). We then examined if Citron-K and KIF14 directly interact. Based on the previously shown interaction between Citron-K and KIF14 C-terminus (Gruneberg et al., 2006) and also on our own finding that GFP-Citron-KΔN (429–2055 aa) co-precipitated the C-terminal KIF14 fragments of amino acids 901–1648 but not 1233–1648 (Fig. 6A;

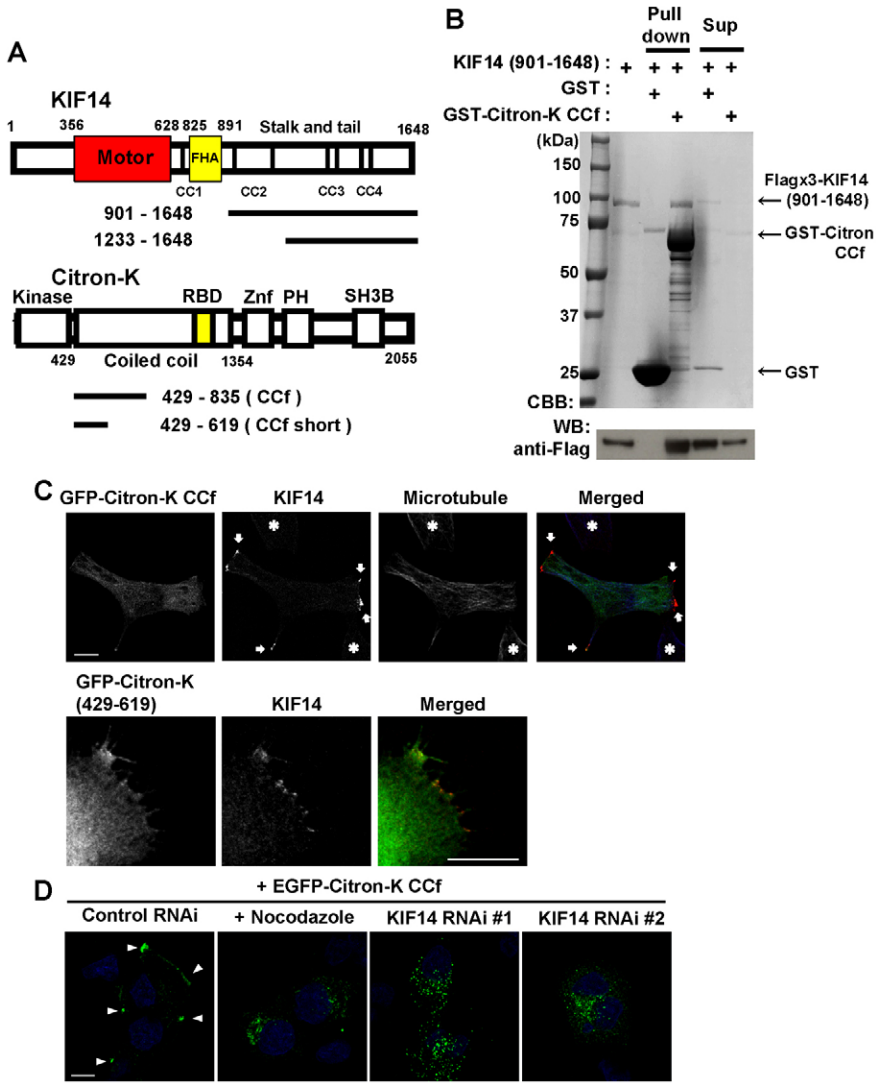

Fig. 6. Citron-K CCf directly binds the 2nd CC domain of KIF14 and regulates its localization. (**A**) Representation of KIF14 and Citron-K. FHA, Forkhead-associated domain. Kinase, kinase domain; RBD, Rho binding domain; Znf, Zn finger domain; PH, pleckstrin homology domain; SH3B, putative SH3-binding domain. Thick lines show fragments used in experiments. (**B**) Direct interaction between KIF14 and CCf. Recombinant FLAGx3-KIF14 (901–1648) was incubated with GSH-Sepharose beads conjugated with either GST or GST-CCf, and the precipitates analyzed by Coomassie staining and immunoblotting. (**C**) Localization of endogenous KIF14 in HeLa cells expressing Citron-K CCf. HeLa cells were transfected with EGFP-Citron-K CCf or EGFP-Citron-K (429–619), and subjected to immunofluorescence for GFP (green), KIF14 (red) and α-tubulin (blue). Asterisks indicate non-transfected cells. Arrows indicate peripheral localization of KIF14. (**D**) Effects of KIF14 RNAi and nocodazole treatment on localization of EGFP-Citron-K CCf. HeLa cells were transfected with EGFP-Citron-K CCf. At 16 hours after transfection, the cells were subjected to control RNAi or KIF14 RNAi. At 24 hours after RNAi transfection, the control RNAi cells were further treated with or without 33 μM nocodazole for 15 minutes. The cells were then fixed with PFA containing 0.2% Triton-X 100, and stained for GFP (green) and DNA (blue). Arrowheads represent accumulation of EGFP-Citron-K at the cell periphery. Note that the peripheral accumulation of CCf became clear with permeabilization during fixation. Scale bars: 10 μm (C), 5 μm (D).

Journal of Cell Science

supplementary material Fig. S8B), we purified recombinant GST-tagged CCf and FLAG-tagged KIF14 (901–1648), and performed a pull-down assay (Fig. 6B). We found that FLAGx3-KIF14 (901–1648) was pulled down with GST-CCf, but not with control GST (Fig. 6B). We also confirmed that GST-CCf pulled down FLAGx3-KIF14 (911–1244) (data not shown). These results suggest that Citron-K CCf directly interacts with the 2nd coiled-coil domain of KIF14 (Fig. 6A). To test whether this interaction functions in cells, we expressed Citron-K CCf or a shorter CCf fragment of amino acids 429–619 in interphase cells, and examined its effect on localization of endogenous KIF14 (Fig. 6C). While immunofluorescence signals for KIF14 were quite low and no particular distribution was found in control cells (Fig. 6C, asterisks), KIF14 accumulated at the cell periphery in Citron-K CCf-expressing cells, and its colocalization with CCf was evident in cells expressing the shorter CCf fragment (Fig. 6C arrows; Fig. 6D). The peripheral accumulation of KIF14 and its colocalization with CCf was confirmed by co-expressing GFP-KIF14 and mCherry-CCf in NIH 3T3 cells (supplementary material Fig. S8C). The peripheral localization of EGFP-Citron-K CCf in turn was diminished by depletion of KIF14 or treatment with nocodazole (Fig. 6D), indicating that Citron-K is delivered or anchored in a manner dependent on KIF14 and microtubules. Notably, we did not observe colocalization of KIF14 and wild type EGFP-Citron-K, but observed that with EGFP-Citron-K FL KD, a kinase-dead mutant of Citron-K (supplementary material Fig. S8E). This may be consistent with the finding by Gruneberg et al. (Gruneberg et al., 2006) that Citron-K KD binds to KIF14 more strongly than wild type. These results together suggest that regulation of the interaction between KIF14 and Citron-K is important for Citron-K localization to exert its function.

Interaction between KIF14 and Citron-K regulates the spatiotemporal transfer of Citron-K to the midbody

To test whether the interaction between KIF14 and Citron-K is important for cytokinesis, we first depleted KIF14 and examined the Citron-K localization in cytokinesis (Fig. 7A). Depletion of KIF14 induced cytokinesis failure in the terminal phase as reported previously (Carleton et al., 2006; Gruneberg et al., 2006) (data not shown). KIF14-RNAi did not affect Citron-K localization at the cleavage furrow in early telophase (Fig. 7A, left), but severely affected its localization at the midbody in late telophase (Fig. 7A, right). These results suggest that KIF14 is important for transfer of Citron-K to the midbody. To further clarify the function of the KIF14–Citron-K interaction in cytokinesis, we examined localization of a Citron-K construct lacking the KIF14-binding region, EGFP-Citron-KΔ(430–618), in cytokinesis (Fig. 7B). In this experiment, cells were synchronized and transfected with siRNACitron-K#1 together with EGFP-Citron-K FL or Δ(430–618), and the localization of GFP signals in telophase was examined. In mid telophase, the percentages of cells that showed the midbody localization were 65.5%±9.5 and 7.7%±4.8% for FL (N=32) and for Δ(430–618) (N=32), respectively. Citron-KΔ(430–618) mostly accumulated

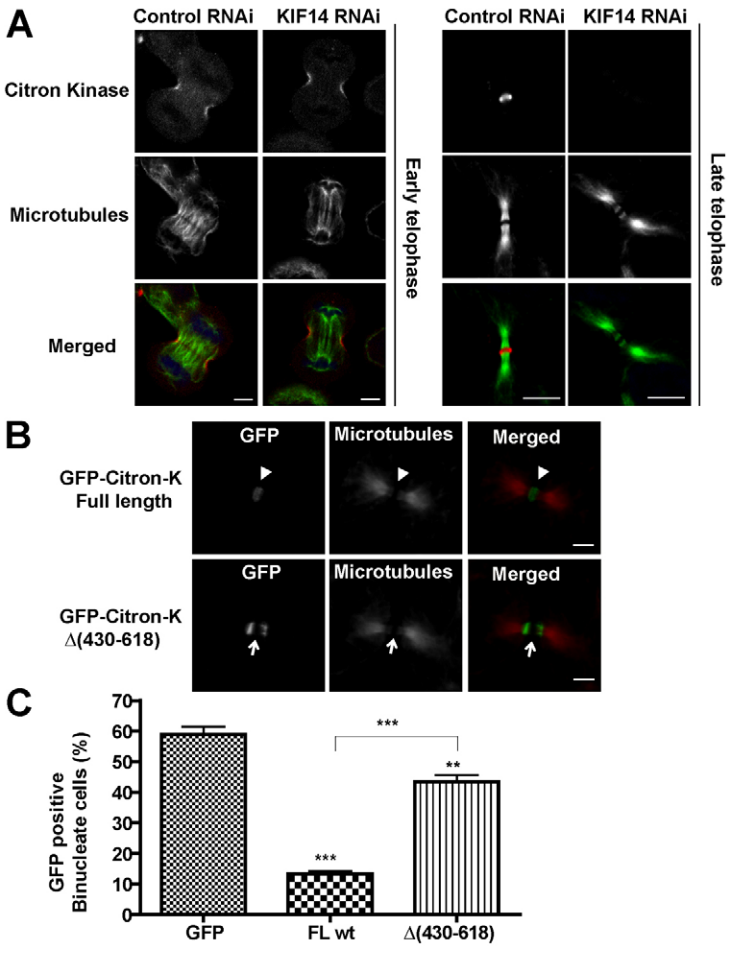

Fig. 7. Interaction between KIF14 and Citron-K CCf regulates the transfer and function of Citron-K in cytokinesis. (**A**) Effects of KIF14 depletion on the transfer of Citron-K from the cleavage furrow onto the midbody. HeLa cells were subjected to control or KIF14 RNAi. At 24 hours after transfection, the cells were fixed and stained for Citron-K (red), α-tubulin (green) and DNA (blue). Cells in early and late telophase are shown at left and right, respectively. (**B**) Localization of Citron-K lacking the KIF14 binding region in cytokinesis. HeLa cells were synchronized and sequentially transfected with siRNAcitron-K#1 and then with either pΔCMV-EGFP-Citron-K FL or Δ(430–618) as described in Fig. 4B. The cells were further enriched in mitosis with nocodazole, and released in fresh medium for 60 minutes. Cells in mid telophase were fixed and stained for GFP (green) and α-tubulin (red). Arrows and arrowheads indicate the lack and presence of GFP signals in the midbody, respectively. (**C**) Impaired rescue of the cytokinesis failure with Citron-K lacking the KIF14 binding region in Citron-K RNAi cells. Experiments were performed as described for Fig. 4C with the indicated constructs. Values indicate percentage of binucleate cells per total cells expressing GFP. The graph shows the mean of more than three independent experiments, in each of which n>100 cells were examined. Error bars indicate s.e.m.; ***P<0.001, **P<0.01 versus GFP by Tukey–Kramer multiple comparison test. Scale bars: 5 μm.

Journal of Cell Science

as two foci at a region neighboring the midbody (Fig. 7B). Conversely, EGFP-Citron-K FL KD that co-localizes with KIF14 in the periphery in interphase cells could accumulate at the midbody when expressed in mitotic Citron-K RNAi cells (data not shown). These results suggest that the interaction between KIF14 and Citron-K is required for the proper spatiotemporal transfer of Citron-K to the midbody. To further validate the importance of the KIF14–Citron-K interaction in cytokinesis, we performed RNAi rescue experiments with GFP-Citron-K Δ(430–618), and found that the phenotype rescue was severely impaired in the cells expressing GFP-Citron-KΔ(430–618) (Fig. 7C). Furthermore, expression of the KD mutant of Citron-K rescued the Citron-K RNAi cytokinesis phenotype only partially (supplementary material Fig. S8F) as seen in the previous report (Bassi et al., 2011). These results collectively suggest that the KIF14–Citron-K interaction is required for Citron-K localization at the midbody and the function of Citron-K in cytokinesis, but that this interaction alone cannot accomplish cytokinesis fully.

Discussion

Here we found that Citron-K depletion induces cytokinesis failure after cleavage furrow ingression (Fig. 1). Citron-K first localizes at the equatorial cell cortex, and then at the cleavage furrow, and forms a ring-like structure at the midbody after the complete furrow ingression (Fig. 2A). FRAP study indicates that, once formed, the ring-like structure is static without any turnover, while Citron-K in the equatorial cell cortex is exchangeable (Fig. 2B). Depletion of Citron-K affects the maintenance of RhoA, Anillin, and septins at the intercellular bridge and midbody in mid–late telophase (Fig. 2C,D; supplementary material Fig. S2B), and the concentration and maintenance of KIF14 and PRC1 in the midbody in late telophase (Fig. 3A,B). Finally, Citron-K CC is critical for the localization and function of Citron-K in cytokinesis, whereas the kinase domain is dispensable (Fig. 4). In CC domain, CCr is important for localization and accumulation of Citron-K at the cleavage furrow through binding to RhoA, and mediates the ring formation in the midbody (Fig. 5), while CCf directly binds KIF14 (Fig. 6), and this interaction mediates the timely transfer of Citron-K to the forming midbody (Fig. 7). Our findings thus uncovered the unexplored control mechanism of the transition between constriction and abscission by Citron-K, and identified critical domains of Citron-K in these actions.

First, the cytokinesis failure induced by Citron-K depletion mostly occurs around 60 minutes after the full furrow ingression (Fig. 1A,C) when the daughter cells are still round, and the failure is observed as one of the daughter cells being absorbed into the other (Fig. 1C; supplementary material Movie 2). Considering that Citron-K forms a ring-like structure, one plausible role for Citron-K is that it tightly packs the midbody microtubules to prevent the microtubules from being pulled into one of the daughter cells. In addition to this ‘early fusion’, a small population of Citron-K RNAi cells exhibited cytokinesis failure 2.5 hours after the full furrow ingression (Fig. 1A,D; supplementary material Movie 3). Since asymmetric microtubule disassembly occurred before this time in most of control RNAi cells (Fig. 1A), the depletion of Citron-K was suspected to affect the abscission machinery. Consistently, the percentage of Citron-K RNAi cells showing asymmetrical disassembly of the midbody microtubules was much smaller than that of control cells (Fig. 3C). Since we did not observe any defect in recruitment of major ESCRT molecules to the midbody (supplementary material Fig. S3B,F), the depletion of Citron-K might cause dysfunction of the ESCRT machinery (Guizetti and Gerlich, 2012). Intriguingly, depletion of ESCRT machinery causes detachment of membrane from the center of the midbody (Morita et al., 2007; Morita et al., 2010), a phenotype similar to the late fusion in Citron-K RNAi cells. Because signals for acetylated tubulin were retained on both sides of the cytoplasmic bridge in Citron-K RNAi cells (Fig. 3C), hyper-stabilization of microtubules caused by Citron-K RNAi may interfere with the abscission machinery as suggested previously (Wickström et al., 2010; Florindo et al., 2012).

Second, we found that Citron-K controls localization of RhoA, Anillin and septins at the intercellular bridge in mid to late telophase (Fig. 2C,D). Although dependence of the Anillin and RhoA localization in this structure on Citron-K was already reported (Echard et al., 2004; Naim et al., 2004; Bassi et al., 2011; Gai et al., 2011), we noticed that these molecules gradually disappear from there in mid to late telophase in control cells (Fig. 2C,D; supplementary material Fig. S2A). These findings suggest that Citron-K maintains their transitional stay in the bridge. Depletion of either Anillin or septins induces cytokinesis impairment similar to that found in Citron-K RNAi cells (Echard et al., 2004; Joo et al., 2007), and the functional link between the two was recently shown by domain-based rescue experiments (Echard et al., 2004; Joo et al., 2007; Kechad et al., 2012). Since septin complex has been reported to be involved in the stabilization of the midbody (Kinoshita et al., 1997; Kechad et al., 2012), Citron-K-mediated control of localization of septin complex in the intercellular bridge might be one of the mechanisms ensuring proper abscission (Fig. 2C). Here we also found that KIF14 concentrates onto the center of the midbody in late telophase in a Citron-K dependent manner (Fig. 3A; supplementary material Fig. S3C–E). Since KIF14 remains there during abscission (supplementary material Fig. S3C,D), this focal concentration of KIF14 may contribute to the proper accumulation of its binding molecules required for abscission. One of such candidates is PRC1. Indeed, Citron-K depletion induced dispersion of PRC1 from the midbody in late telophase (Fig. 3B; supplementary material Movie 6). Fly homologues of KIF14 and PRC1 have been reported to be involved in lateral crosslink between microtubules (Noguchi et al., 2011). These results therefore suggest that Citron-K stabilizes KIF14–PRC1 complex in the midbody for bundling microtubules. On this hypothesis, debundling of microtubules by Citron-K RNAi is induced by failure in proper accumulation of this KIF14–PRC1 complex, and is the cause of abscission error. Alternatively, disintegration of the midbody microtubules by the absence of the ring-like structure of Citron-K may lead to the scattering of PRC1. It is also possible that the two mechanisms function collaboratively.

Third, cytokinesis failure by Citron-K RNAi was effectively rescued with its CC domain, and both its kinase domain and C-terminal domain are dispensable (Fig. 4). Our study has thus verified without ambiguity the earlier suggestion by Dean and Spudich (Dean and Spudich, 2006) that Citron-K controls cytokinesis in a myosin-phosphorylation independent manner. We further clarified region-specific roles of the CC domain in cytokinesis by characterization of the two distinct parts of CC, CCf and CCr (Figs 5–7). CCr contains RBD, and its deletion or

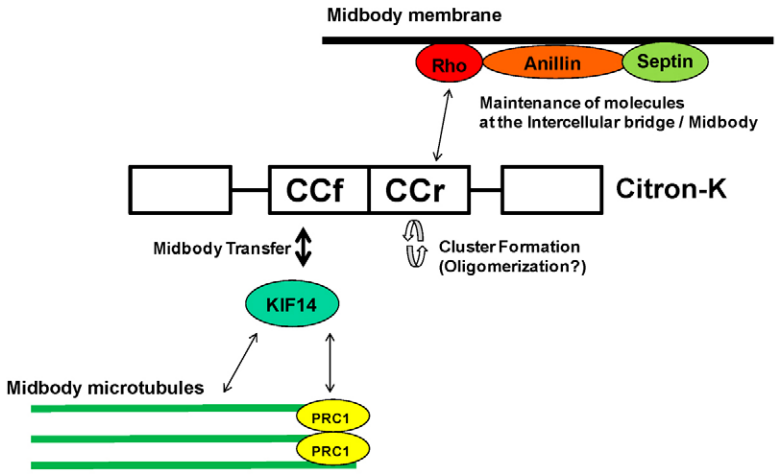

Fig. 8. Model for the action of Citron-K in cytokinesis. For details see text.

mutation in RBD decreased the localization at the cleavage furrow and the midbody (Fig. 5B,C). Therefore, Rho functions as a carrier of Citron-K from the cleavage furrow to the intercellular bridge by binding to the CCr domain. Another important region in CCr essential for the Citron-K function is the region of amino acids 1140–1213 (Fig. 5A). A Citron-K fragment lacking this region, CCrΔ71, exhibited localization at the cleavage furrow, but not at the midbody (Fig. 5B,E), which suggests that Citron-K requires this region to accumulate at the midbody in addition to RBD. We found that this region has high homology to that observed in the CC domain of MKLP1/KIF23 (supplementary material Fig. S7B). Previously, this region of a worm orthologue of MKLP1/KIF23 was shown to mediate its clustering (Hutterer et al., 2009). Since MKLP1 and Citron-K exhibit similar accumulation in the midbody (supplementary material Fig. S3A), these proteins may share a similar clustering mechanism. Indeed, CCr but not CCrΔ71 forms clusters, when expressed in interphase cells (Fig. 5E). Intriguingly, FRAP study showed negligible turnover of Citron-K molecules in these clusters (supplementary material Fig. S7A), which is similar to that found in the Citron-K ring at the midbody (supplementary material Fig. S1) (Fig. 2B). Given that CCr but not CCrΔ71 forms a ring in the midbody, these results suggest that cluster-forming activity mediates formation of the ring of Citron-K at the midbody.

Another important region of CC, CCf, directly binds to KIF14 (Fig. 6B). This interaction between Citron-K and KIF14 is important not only for Citron-K localization at the midbody, but also for that of KIF14. Expression of CCf induced peripheral accumulation of endogenous KIF14 (Fig. 6C), and this localization pattern is similar to that of active mutant of KIF17, which contains a mutation that abolishes the auto-inhibition of KIF17 (Jaulin and Kreitzer, 2010). Considering that the region binding to Citron-K CCf resides in the second CC domain in KIF14 tail region, the interaction between CCf and KIF14 may liberate KIF14 from its closed inactive state, and induce accumulation in the cells by possibly activating its motility as seen in KIF17. Based on these findings, we propose our working model for the function of Citron-K during cytokinesis (Fig. 8). Citron-K localizes at the cleavage furrow through interaction between CCr and RhoA, and stays there until full ingression. This interaction via CCr also enables Citron-K to maintain RhoA, Anillin, and septin complex at the intercellular bridge. Upon accumulation on the intercellular bridge, Citron-K interacts with KIF14 through CCf, and through this interaction, Citron-K is timely transfered into the midbody after completion of the furrow ingression. After its transfer into the midbody, Citron-K forms a ring-like structure through cluster-forming activity of CCr. Overall, these multifunctional activities of Citron-K CC domain ensure proper transition from constriction to abscission.

Materials and Methods

Materials

Antibodies and siRNAs used in this study were described in supplementary material Tables S1, S2. Constructs used in this study were prepared by PCR amplification of corresponding sequences and restriction enzyme digestion as shown in supplementary material Table S3.

Cell culture and transfection

NIH 3T3, HeLa, and HEK293F cells were maintained as described previously (Watanabe et al., 2010). EGFP-tub HeLa cells were isolated as follows. pEGFP-αTubulin was linearized and transfected into HeLa cells. At 24 hours after transfection, 0.8 mg/ml of G418 (Invitrogen) was added. After 3 days of incubation, the cells were re-plated, and individual clones were selected. Transfection was performed using LipofectamineRNAiMAX (Invitrogen) and FreeStyleMAX (Invitrogen) as described previously (Watanabe et al., 2010). Transfection of plasmids with Neon Transfection System (Invitrogen) was performed according to the manufacturer's protocol with a single pulse of 1050 V and 35 milliseconds. Sequential transfection of siRNAs and plasmids was performed as follows. HeLa cells were seeded and cultured with DMEM containing 10 mM thymidine for 14 hours. The cells were then washed twice with PBS and subjected to RNAi transfection. The transfected cells were further cultured in fresh culture medium for 8–10 hours. The medium was then replaced again with culture medium containing 10 mM thymidine and the cells were cultured for another 14 hours. The cells were trypsinized and transfected with plasmids, and further cultured for 11 or 16 hours in fresh medium before being fixed for immunofluorescence. For synchronization in mitotic phases, the transfected cells were cultured in the medium alone for 8 hours after the 2nd thymidine block and for another 4 hours in that containing 20 ng/ml nocodazole (Biomol). The cells were then washed free of nocodazole and further cultured for 60, 90 and 120 minutes before being fixed for immunofluorescence.

Fluorescence microscopy

Cells were plated in a 35-mm culture dish, and fixed with paraformaldehyde (PFA) or trichloroacetic acid and stained as described previously (Watanabe et al., 2008) using antibodies listed in supplementary material Table S2. Staining was examined with Leica SP5 confocal imaging system (Plan-Apo 63×, NA 1.40). The images were analyzed by MetaMorph software (Molecular Devices). Quantification of signal intensities in supplementary material Fig. S2B, Fig. S5D and Fig. S6C was performed using the 'line scan' function in MetaMorph as described previously (Watanabe et al., 2010). An image of the middle section of each telophase cell was used for analysis. The background signals outside the cell were averaged and subtracted from each image before analysis. Line scans with a width of 5 pixels and a length of 100 pixels were performed perpendicular to the longitudinal axis of cells at the center of the microtubule gap region as shown in supplementary material Fig. S2B. Maximum values of the averaged line scan intensities were obtained as 'signals at center of the intercellular bridge'. For live imaging, cells

Journal of Cell Science

Journal of Cell Science

were plated onto glass-bottom dishes (Matsunami) coated with 100 μg/ml poly-L-lysine. The dish was then placed on a temperature-controlled stage maintained at 37℃ with 5% CO_2. For Fig. 1 and Fig. 3B, EGFP-tub HeLa cells transfected either with or without mCherry-PRC1 were imaged on the Leica SP5 microscope (HCX-PLANAPO-CS 100×, NA 1.40) every 30 seconds or 2 minutes for 1.5–3 hours. FRAP experiments were performed with Olympus FV1000 confocal microscope (UPLASAPO, 60×, NA 1.35) (Uehara et al., 2010). Images were acquired every 2 seconds. After obtaining the initial five frames, GFP signals in a rectangle region of interest (60×30 pixels) were photobleached for 2 seconds using a 488 nm laser (30 mw, 20%).

Immunoprecipitation GST pull-down analysis

For immunoprecipitation in supplementary material Fig. S8B, 1.0×10^7 HEK293F cells expressing GST-FLAGx3-tagged and GFP-tagged proteins were harvested by centrifugation and lysed in 1 ml of lysis buffer containing 20 mM Tris-HCl, pH 7.5, 100 mM NaCl, 1 mM EDTA, 1 mM dithiothreitol, 1% NP-40, 0.1% deoxycholate, and 'Complete' protease inhibitor cocktail (Roche) for 15 minutes on ice. Cell lysates were centrifuged, and the supernatants were incubated with 20 μl of anti-GFP antibody conjugated-agarose beads (MBL) for 2 hours at 4℃. The beads were then washed three times with the lysis buffer and eluted with Laemmli sample buffer. Eluted samples were analyzed by SDS-PAGE and immunoblotting.

For the pull-down experiment in Fig. 6B and supplementary material Fig. S5B, GST-Citron-K CCf and GST-RhoA expression plasmids were introduced in *Escherichia coli* BL21 (DE3) (Novagen). GST fusion proteins were then expressed and purified as described previously (Watanabe et al., 2010). For Fig. 6B, 6.0×10^7 HEK293F cells expressing GST-FLAGx3-KIF14 (901–1648) were harvested and lysed as above. The supernatant was incubated with 100 μl of glutathione-Sepharose 4 fast flow (GSH) beads (GE Healthcare) for 2 hours at 4℃. The beads were washed with the lysis buffer containing 500 mM NaCl, and then incubated in 400 μl of PBS containing 1 mM dithiothreitol (D-PBS) with 4 U of PreScission protease (GE Healthcare) for 16 hours at 4℃. After cleaved GST-GSH beads and precision protease were removed, 150 μl of the supernatant containing FLAGx3-KIF14 (901–1648) was incubated with 30 μl of GSH-beads and either 60 μg of GST or 30 μg of GST-Citron-K CCf for 2 hours at 4℃. The beads were washed three times with D-PBS containing 0.02% Tween-20 and the protein complex was analyzed by SDS-PAGE, Coomassie staining, and Western blotting.

For supplementary material Fig. S5B, 4.0×10^7 HEK293F cells expressing GFP, GFP-Citron-K CC, GFP-Citron-K CC L1263N were harvested and resuspended in lysis buffer containing 25 mM Tris-HCl, pH 7.5, 100 mM NaCl, 5 mM $MgCl_2$, 1 mM dithiothreitol, 0.05% Tween-20 with brief sonication. The cell lysates were then centrifuged and precleared by GSH beads. In parallel, GST-RhoA were loaded with 150 μM guanosine 5′-[γ-thio]triphosphate (GTPγS) as described previously (Watanabe et al., 2010). The precleared cell lysates were incubated with 100 μg of the GTPγS loaded GST-RhoA and 20 μl of GSH-beads for 1 hour at 4℃. The beads were washed three times with the lysis buffer, and the protein complex was analyzed by SDS-PAGE, Coomassie staining, and Western blotting.

Statistical analysis

Data are presented as mean ± s.d. or s.e.m., and were evaluated using one-way ANOVA and tests indicated in the figure legends. $P<0.05$ was considered statistically significant.

Acknowledgements

We thank K. Nonomura, A. Washimi, and T. Arai for assistance, M. Kinoshita, M. Maki, G. Goshima, R. Uehara of Nagoya University, and N. Watanabe of Tohoku University for reagents and helpful discussions.

Author contributions

S.W. designed the study and carried out most of the experiments and co-wrote the manuscript. T.D.Z. helped experiments and analyses in Fig. 3-6. T.I carried out some of the experiments related to Fig. 5-6. S.N. co-wrote the manuscript. S.W and S.N. are co-corresponding authors. T.I and S.N. supervised the project.

Funding

This work was supported by Grants-in-Aid for Scientific Research [grant numbers 23121514 and 23229003] from MEXT of Japan. S.W. was supported by JSPS Research fellowships.

Supplementary material available online at
http://jcs.biologists.org/lookup/suppl/doi:10.1242/jcs.116608/-/DC1

References

Barr, F. A. and Gruneberg, U. (2007). Cytokinesis: placing and making the final cut. *Cell* **131**, 847-860.

Bassi, Z. I., Verbrugghe, K. J., Capalbo, L., Gregory, S., Montembault, E., Glover, D. M. and D'Avino, P. P. (2011). Sticky/Citron kinase maintains proper RhoA localization at the cleavage site during cytokinesis. *J. Cell Biol.* **195**, 595-603.

Blumenstein, L. and Ahmadian, M. R. (2004). Models of the cooperative mechanism for Rho effector recognition: implications for RhoA-mediated effector activation. *J. Biol. Chem.* **279**, 53419-53426.

Caballe, A. and Martin-Serrano, J. (2011). ESCRT machinery and cytokinesis: the road to daughter cell separation. *Traffic* **12**, 1318-1326.

Carleton, M., Mao, M., Biery, M., Warrener, P., Kim, S., Buser, C., Marshall, C. G., Fernandes, C., Annis, J. and Linsley, P. S. (2006). RNA interference-mediated silencing of mitotic kinesin KIF14 disrupts cell cycle progression and induces cytokinesis failure. *Mol. Cell. Biol.* **26**, 3853-3863.

Cunto, F. D., Imarisio, S., Camera, P., Boitani, C., Altruda, F. and Silengo, L. (2002). Essential role of citron kinase in cytokinesis of spermatogenic precursors. *J. Cell Sci.* **115**, 4819-4826.

D'Avino, P. P., Savoian, M. S. and Glover, D. M. (2004). Mutations in sticky lead to defective organization of the contractile ring during cytokinesis and are enhanced by Rho and suppressed by Rac. *J. Cell Biol.* **166**, 61-71.

Dean, S. O. and Spudich, J. A. (2006). Rho kinase's role in myosin recruitment to the equatorial cortex of mitotic Drosophila S2 cells is for myosin regulatory light chain phosphorylation. *PLoS ONE* **1**, e131.

Di Cunto, F., Calautti, E., Hsiao, J., Ong, L., Topley, G., Turco, E. and Dotto, G. P. (1998). Citron rho-interacting kinase, a novel tissue-specific ser/thr kinase encompassing the Rho-Rac-binding protein Citron. *J. Biol. Chem.* **273**, 29706-29711.

Di Cunto, F., Imarisio, S., Hirsch, E., Broccoli, V., Bulfone, A., Migheli, A., Atzori, C., Turco, E., Triolo, R., Dotto, G. P. et al. (2000). Defective neurogenesis in citron kinase knockout mice by altered cytokinesis and massive apoptosis. *Neuron* **28**, 115-127.

Dvorsky, R., Blumenstein, L., Vetter, I. R. and Ahmadian, M. R. (2004). Structural insights into the interaction of ROCKI with the switch regions of RhoA. *J. Biol. Chem.* **279**, 7098-7104.

Echard, A., Hickson, G. R., Foley, E. and O'Farrell, P. H. (2004). Terminal cytokinesis events uncovered after an RNAi screen. *Curr. Biol.* **14**, 1685-1693.

Eda, M., Yonemura, S., Kato, T., Watanabe, N., Ishizaki, T., Madaule, P. and Narumiya, S. (2001). Rho-dependent transfer of Citron-kinase to the cleavage furrow of dividing cells. *J. Cell Sci.* **114**, 3273-3284.

Eggert, U. S., Mitchison, T. J. and Field, C. M. (2006). Animal cytokinesis: from parts list to mechanisms. *Annu. Rev. Biochem.* **75**, 543-566.

Elad, N., Abramovitch, S., Sabanay, H. and Medalia, O. (2011). Microtubule organization in the final stages of cytokinesis as revealed by cryo-electron tomography. *J. Cell Sci.* **124**, 207-215.

Florindo, C., Perdigão, J., Fesquet, D., Schiebel, E., Pines, J. and Tavares, A. A. (2012). Human Mob1 proteins are required for cytokinesis by controlling microtubule stability. *J. Cell Sci.* **125**, 3085-3090.

Fujita, A., Shishido, T., Yuan, Y., Inamoto, E., Narumiya, S., Watanabe, N. (2009). Imatinib mesylate (STI571)-induced cell edge translocation of kinase-active and kinase-defective Abelson kinase: requirements of myristoylation and src homology 3 domain. *Mol. Pharmacol.* **75**, 75-84.

Gai, M., Camera, P., Dema, A., Bianchi, F., Berto, G., Scarpa, E., Germena, G. and Di Cunto, F. (2011). Citron kinase controls abscission through RhoA and anillin. *Mol. Biol. Cell* **22**, 3768-3778.

Gruneberg, U., Neef, R., Li, X., Chan, E. H., Chalamalasetty, R. B., Nigg, E. A. and Barr, F. A. (2006). KIF14 and citron kinase act together to promote efficient cytokinesis. *J. Cell Biol.* **172**, 363-372.

Guizetti, J. and Gerlich, D. W. (2012). ESCRT-III polymers in membrane neck constriction. *Trends Cell Biol.* **22**, 133-140.

Guizetti, J., Schermelleh, L., Mäntler, J., Maar, S., Poser, I., Leonhardt, H., Müller-Reichert, T. and Gerlich, D. W. (2011). Cortical constriction during abscission involves helices of ESCRT-III-dependent filaments. *Science* **331**, 1616-1620.

Guse, A., Mishima, M. and Glotzer, M. (2005). Phosphorylation of ZEN-4/MKLP1 by aurora B regulates completion of cytokinesis. *Curr. Biol.* **15**, 778-786.

Higashida, C., Miyoshi, T., Fujita, A., Oceguera-Yanez, F., Monypenny, J., Andou, Y., Narumiya, S., Watanabe, N. (2004). Actin polymerization-driven molecular movement of mDia1 in living cells. *Science* **303**, 2007-2010.

Hu, C. K., Coughlin, M. and Mitchison, T. J. (2012). Midbody assembly and its regulation during cytokinesis. *Mol. Biol. Cell* **23**, 1024-1034.

Hutterer, A., Glotzer, M. and Mishima, M. (2009). Clustering of centralspindlin is essential for its accumulation to the central spindle and the midbody. *Curr. Biol.* **19**, 2043-2049.

Jaulin, F. and Kreitzer, G. (2010). KIF17 stabilizes microtubules and contributes to epithelial morphogenesis by acting at MT plus ends with EB1 and APC. *J. Cell Biol.* **190**, 443-460.

Joo, E., Surka, M. C. and Trimble, W. S. (2007). Mammalian SEPT2 is required for scaffolding nonmuscle myosin II and its kinases. *Dev. Cell* **13**, 677-690.

Kechad, A., Jananji, S., Ruella, Y. and Hickson, G. R. (2012). Anillin acts as a bifunctional linker coordinating midbody ring biogenesis during cytokinesis. *Curr. Biol.* **22**, 197-203.

Kinoshita, M., Kumar, S., Mizoguchi, A., Ide, C., Kinoshita, A., Haraguchi, T., Hiraoka, Y. and Noda, M. (1997). Nedd5, a mammalian septin, is a novel

cytoskeletal component interacting with actin-based structures. *Genes Dev.* **11**, 1535-1547.

Lee, H. H., Elia, N., Ghirlando, R., Lippincott-Schwartz, J. and Hurley, J. H. (2008). Midbody targeting of the ESCRT machinery by a noncanonical coiled coil in CEP55. *Science* **322**, 576-580.

Madaule, P., Eda, M., Watanabe, N., Fujisawa, K., Matsuoka, T., Bito, H., Ishizaki, T. and Narumiya, S. (1998). Role of citron kinase as a target of the small GTPase Rho in cytokinesis. *Nature* **394**, 491-494.

Madaule, P., Furuyashiki, T., Eda, M., Bito, H., Ishizaki, T. and Narumiya, S. (2000). Citron, a Rho target that affects contractility during cytokinesis. *Microsc. Res. Tech.* **49**, 123-126.

Miki, T., Kamikawa, Y., Kurono, S., Kaneko, Y., Katahira, J., Yoneda, Y. (2011). Cell type-dependent gene regulation by Staufen2 in conjunction with Upf1. *BMC Mol. Biol.* **12**, 48.

Morita, E., Sandrin, V., Chung, H. Y., Morham, S. G., Gygi, S. P., Rodesch, C. K. and Sundquist, W. I. (2007). Human ESCRT and ALIX proteins interact with proteins of the midbody and function in cytokinesis. *EMBO J.* **26**, 4215-4227.

Morita, E., Colf, L. A., Karren, M. A., Sandrin, V., Rodesch, C. K. and Sundquist, W. I. (2010). Human ESCRT-III and VPS4 proteins are required for centrosome and spindle maintenance. *Proc. Natl. Acad. Sci. USA* **107**, 12889-12894.

Naim, V., Imarisio, S., Di Cunto, F., Gatti, M. and Bonaccorsi, S. (2004). Drosophila citron kinase is required for the final steps of cytokinesis. *Mol. Biol. Cell* **15**, 5053-5063.

Narumiya, S. and Yasuda, S. (2006). Rho GTPases in animal cell mitosis. *Curr. Opin. Cell Biol.* **18**, 199-205.

Neto, H. and Gould, G. W. (2011). The regulation of abscission by multi-protein complexes. *J. Cell Sci.* **124**, 3199-3207.

Noguchi, T., Koizumi, M. and Hayashi, S. (2011). Sustained elongation of sperm tail promoted by local remodeling of giant mitochondria in Drosophila. *Curr. Biol.* **21**, 805-814.

Paramasivam, M., Chang, Y. J. and LoTurco, J. J. (2007). ASPM and citron kinase co-localize to the midbody ring during cytokinesis. *Cell Cycle* **6**, 1605-1612.

Piekny, A., Werner, M. and Glotzer, M. (2005). Cytokinesis: welcome to the Rho zone. *Trends Cell Biol.* **15**, 651-658.

Pollard, T. D. (2010). Mechanics of cytokinesis in eukaryotes. *Curr. Opin. Cell Biol.* **22**, 50-56.

Serres, M. P., Kossatz, U., Chi, Y., Roberts, J. M., Malek, N. P. and Besson, A. (2012). p27(Kip1) controls cytokinesis via the regulation of citron kinase activation. *J. Clin. Invest.* **122**, 844-858.

Shandala, T., Gregory, S. L., Dalton, H. E., Smallhorn, M. and Saint, R. (2004). Citron kinase is an essential effector of the Pbl-activated Rho signalling pathway in Drosophila melanogaster. *Development* **131**, 5053-5063.

Shimizu, T., Ihara, K., Maesaki, R., Amano, M., Kaibuchi, K. and Hakoshima, T. (2003). Parallel coiled-coil association of the RhoA-binding domain in Rho-kinase. *J. Biol. Chem.* **278**, 46046-46051.

Steigemann, P. and Gerlich, D. W. (2009). Cytokinetic abscission: cellular dynamics at the midbody. *Trends Cell Biol.* **19**, 606-616.

Subramanian, R., Wilson-Kubalek, E. M., Arthur, C. P., Bick, M. J., Campbell, E. A., Darst, S. A., Milligan, R. A. and Kapoor, T. M. (2010). Insights into antiparallel microtubule crosslinking by PRC1, a conserved nonmotor microtubule binding protein. *Cell* **142**, 433-443.

Suzuki, H., Kawasaki, M., Inuzuka, T., Okumura, M., Kakiuchi, T., Shibata, H., Wakatsuki, S., Maki, M. (2008). Structural basis for Ca2+ -dependent formation of ALG-2/Alix peptide complex: Ca2+/EF3-driven arginine switch mechanism. *Structure* **16**, 1562-1573.

Uehara, R., Goshima, G., Mabuchi, I., Vale, R. D., Spudich, J. A. and Griffis, E. R. (2010). Determinants of myosin II cortical localization during cytokinesis. *Curr. Biol.* **20**, 1080-1085.

Watanabe, N. (2012). Fluorescence single-molecule imaging of actin turnover and regulatory mechanisms. *Methods Enzymol.* **505**, 219-232.

Watanabe, S., Ando, Y., Yasuda, S., Hosoya, H., Watanabe, N., Ishizaki, T. and Narumiya, S. (2008). mDia2 induces the actin scaffold for the contractile ring and stabilizes its position during cytokinesis in NIH 3T3 cells. *Mol. Biol. Cell* **19**, 2328-2338.

Watanabe, S., Okawa, K., Miki, T., Sakamoto, S., Morinaga, T., Segawa, K., Arakawa, T., Kinoshita, M., Ishizaki, T. and Narumiya, S. (2010). Rho and anillin-dependent control of mDia2 localization and function in cytokinesis. *Mol. Biol. Cell* **21**, 3193-3204.

Wickström, S. A., Masoumi, K. C., Khochbin, S., Fässler, R. and Massoumi, R. (2010). CYLD negatively regulates cell-cycle progression by inactivating HDAC6 and increasing the levels of acetylated tubulin. *EMBO J.* **29**, 131-144.

Yamashiro, S., Totsukawa, G., Yamakita, Y., Sasaki, Y., Madaule, P., Ishizaki, T., Narumiya, S. and Matsumura, F. (2003). Citron kinase, a Rho-dependent kinase, induces di-phosphorylation of regulatory light chain of myosin II. *Mol. Biol. Cell* **14**, 1745-1756.

Yasuda, S., Oceguera-Yanez, F., Kato, T., Okamoto,M., Yonemura, S., Terada, Y., Ishizaki, T., Narumiya, S. (2004). Cdc42 and mDia3 regulate microtubule attachment to kinetochores. *Nature* **428**, 767-771.

Zhang, W. and Benson, D. L. (2006). Targeting and clustering citron to synapses. *Mol. Cell. Neurosci.* **31**, 26-36.

Journal of Cell Science